# Reliability Assessment of Fault-Tolerant Dc-Dc Converters for Photovoltaic Applications

Sairaj V. Dhople, Ali Davoudi, Patrick L. Chapman and Alejandro D. Domínguez-García
Grainger Center for Electric Machinery and Electromechanics
Department of Electrical and Computer Engineering
University of Illinois at Urbana-Champaign
Urbana, Illinois 61801, USA
sdhople2@illinois.edu

***Abstract*— A framework for integrating performance and reliability analysis of switch-mode, dc-dc power converters employed as front ends in photovoltaic energy processing applications is presented. The proposed approach acknowledges the influence of the converter's steady-state operation on device failure rates. Markov reliability models are derived to assess reliability-oriented metrics of the system. The conceptual background is elucidated in the context of a topologically-redundant dc-dc converter, and the dependence of the Mean Time to Failure on design parameters is explored. The subtle affiliation between power-electronics design and system reliability is assessed through several case studies.**

***Index Terms*— Markov reliability modeling, photovoltaic systems, power electronics, reliability.**

## I. INTRODUCTION

Reliability of photovoltaic (PV) energy conversion systems is of paramount concern owing to the high fixed costs of such installations and the mission-critical nature of certain applications, e.g., satellites. Past research in reliability of such systems has primarily focused on PV sources [1]-[2], and only recently have the power-electronic circuits that process the PV output received interest. Part of the attention has been the consequence of increased adoption of grid-tied inverters [3]. Practical considerations from the perspective of balance-of-system components are well detailed in [4]; and in [5], a systematic approach to studying the reliability of power-electronic components in a PV inverter is presented and demonstrated with a real-world example. In [6], a coherent methodology for integrating reliability considerations into the design of fault-tolerant power converters is presented. The proposed approach ensures that state variables are bounded based on performance requirements in the presence of uncontrolled inputs. The non-linear PV source renders such methods mathematically intractable for PV applications.

The theoretical models derived in this work are presented in the context of a multi-phase, interleaved boost converter that delivers power from a PV source to a constant-impedance load. Fig. 1 depicts a three-phase example of this type. Analogous topologically-redundant converter designs are typically used when system reliability is a dominant concern.

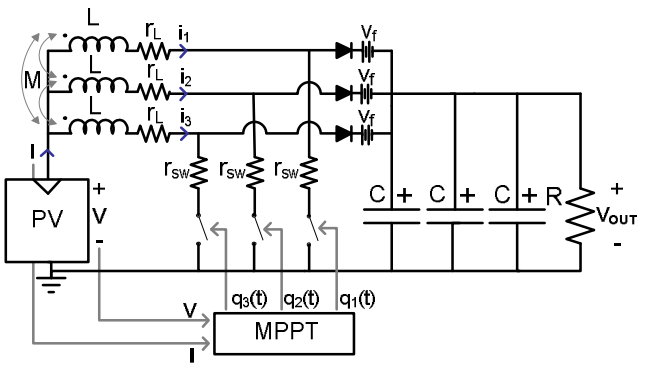


Fig. 1. Three-phase, interleaved boost converter model for PV applications

A circuit topology similar to that considered in this work is analyzed with a reliability-oriented perspective in [7]. It is demonstrated that employing derated semiconductor devices enables the construction of more reliable converters without resorting to soft-switching techniques. References [8]-[9] examine the reliability of different circuit topologies applied to PV applications with the objective of identifying the weakest link in the design. The results indicate that the switching stage is most likely to fail and temperature is revealed as the most likely cause of failure.

Empirically accepted system-level traits generally guide design practices for power-electronic circuitry that process PV energy. For instance, structural redundancy is expected to translate to improved reliability, but, aluminum electrolytic capacitors are regarded unreliable. While these statements could be contextually true, there are undeniable tradeoffs between converter performance and reliability that need to be addressed before finalizing design choices. In particular, the analytical description of the converter is indispensable to quantifying overall system reliability. Factors such as voltage ripple imposed on the capacitor bank and losses in the switching devices establish the failure rates of these devices. Ambient temperature and incident solar

insolation determine the terminal voltage and current sourced by the PV module, and in turn affect the stresses on the various components in the converter. A meaningful reliability assessment hence demands an accurate steady-state description and both aspects are given equal attention in the forthcoming analysis.

## II. Steady-State Characterization of N-Phase, Interleaved Boost Converter

The converter model includes resistance in the inductors ($r_L$) and switches ($r_{SW}$) to model winding losses in the inductors and conduction losses in the switches. Conduction losses in the diodes are modeled by forward voltage drops ($V_f$). A coupled inductor is utilized to improve the static and dynamic performance. Each phase has self inductance, $L$, and is coupled with every other phase with mutual inductance, $M$. The output filter bank of an $N$-phase converter is realized with $N$ capacitors, each with capacitance $C$. For illustrative purposes, the converter processes power from a 230 Watt SPR-230-WHT module [10] and delivers it to a constant impedance load, $R$. The specifications of the PV module are listed in Table I.

TABLE I
Parameters of PV Module: SPR-230-WHT [10]

| Symbol | Quantity | Value |
|---|---|---|
| $V_{OC}$ | Rated open-circuit voltage | 48.7 V |
| $I_{SC}$ | Rated short-circuit current | 5.99 A |
| $I_M$ | Rated current | 5.61 A |
| $V_M$ | Rated voltage | 41 V |
| $P_M$ | Rated power | 230.01 W |
| $\alpha$ | Temp. coefficient for current | 3.5 mA / °C |
| $\beta$ | Temp. coefficient for voltage | -132.5 mV / °C |

In steady state, the average current through each phase is equal. The maximum power point (MPP) tracker operates the PV module at the MPP voltage and current, denoted as $V_M$ and $I_M$, respectively. The average input current, $I$, is then equal to $I_M$ and the average input voltage, $V$, is equal to $V_M$ (refer to Fig. 1). The phase, switch, and diode currents are illustrated in Fig. 2 for a three-phase converter with strong coupling. The periods $D_{SW}T$, and, $D_DT$, refer to the time for which the active switch and diode conduct. As depicted in the figure, $T$, is the switching period, while $f$ denotes the switching frequency.

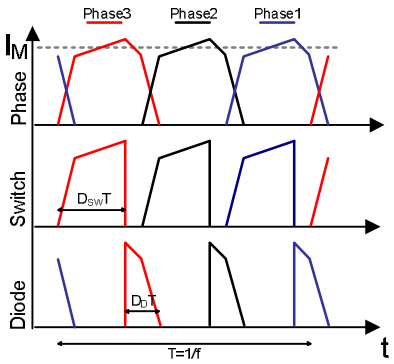

Fig. 2. Current waveforms for a three-phase, interleaved boost converter

The output voltage, $V_{OUT}$, output voltage ripple, $\Delta V_{OUT}$, and power losses in the switching devices, $P_{SW}$, and, $P_D$, are expected to directly impact device failure. The steady-state model of the converter derived in [11] provides the following expressions for these critical quantities:

$$V_{OUT} = IR(1 - D_{SW}N) \tag{1}$$

$$\Delta V_{OUT} = \left( I - \frac{V_{OUT}}{R} \right) \frac{D_{SW}}{fNC} \tag{2}$$

$$P_{SW} = NI^2 r_{SW} D_{SW} \tag{3}$$

$$P_D = NIV_f D_D \tag{4}$$

With strong coupling, the following is guaranteed for an $N$-phase converter:

$$D_{SW} + D_D = 1/N \tag{5}$$

The duty ratio of the active switch, $D_{SW}$, is obtained as the solution to the following quadratic equation:

$$D_{SW}^2 (N^2 I^2 R) + D_{SW} (NI^2 r_{SW} - NIV_f - 2NI^2 R) + (I^2 R - IV + I^2 r_L + IV_f) = 0 \tag{6}$$

## III. Component Failure Rates

The failure-rate models in this work are adopted from the *Military Handbook for Reliability Prediction of Electronic Equipment*, MIL-HDBK-217F [12]. The time-invariant rates proposed in [12] correspond to exponentially-distributed component lifetimes. This is not an over simplification, as large classes of electronic devices are predicted to fail with a constant failure rate over the bulk of their lifetime. Most failure rates in [12] are of the general form:

$$\lambda_P = \lambda_B \pi_E \pi_Q \prod \pi_i \tag{7}$$

In (7), the failure rate, $\lambda_B$, is the base failure rate and $\pi_E$ and $\pi_Q$ are modifiers to account for environmental and qualitative effects. Other device-specific modifiers are denoted as $\pi_i$. The components chosen to realize the converter are listed in Table II. The appropriate sections from [12] that describe the failure rate of each component are attached alongside.

TABLE II
Component Choices and Sections in [12] that Describe Coresponding Failure-Rate Models

| Component | Type | Section |
|---|---|---|
| Active switches | N-Channel silicon power field effect transistors | 6.4 |
| Diodes | Schottky power diodes | 6.1 |
| Capacitors | Dry aluminum electrolytic capacitors | 10.15 |

The failure rate of the inductors is a function of ambient temperature and independent of converter design (e.g., number of phases, switching frequency). Hence, we disregard the failure of the coupled inductor in the following analysis.

The impact of the steady-state performance of the converter on the failure rate of the components is demonstrated for specifications attached in Table III. As a precursor to assessing the overall reliability of an *N*-phase converter, we review the dominant factors that affect each component through simulation runs applicable for specifications in Table III.

TABLE III
COMPONENT CHOICES AND DEVICE RATINGS

| Symbol | Quantity | Value |
|---|---|---|
| $L$ | Self inductance of coupled inductor | 1.2 mH |
| $M$ | Mutual inductance of coupled inductor | 1.18 mH |
| $r_L$ | Winding resistance of each phase | 0.1 Ω |
| $r_{SW}$ | Drain-source ON-state switch resistance | 0.1 Ω |
| $V_f$ | Forward voltage drop of diode | 1 V |
| $C$ | Output capacitance | 4.7 µF |
| $R$ | Output load | 50 Ω |
| $f$ | Switching frequency | 10 kHz |
| $P_{RATING\text{-}SW}$ | Power rating of active switches | 200 W |
| $V_{RATING\text{-}DIODE}$ | Voltage rating of diode | 150 V |
| $\Theta_{JC}$ | Junction-case thermal resistance | 5 W/°C |
| $V_{RATING\text{-}CAP}$ | Voltage rating of capacitor | 100 V |

## A. Capacitors

Fig. 3 depicts the variation of the capacitor failure rate, $\lambda_{CAP}$, as a function of incident insolation, $S$, and ambient temperature, $T$, for different number of phases, $N$. As $N$ increases, the output voltage ripple decreases, and hence, the failure rates drop across all ambient conditions. A common characteristic that Fig. 3 shares with those that follow is the seeming independence of $\lambda_{CAP}$ to temperature except at high insolation levels, and in all cases, the influence of insolation is dominant.

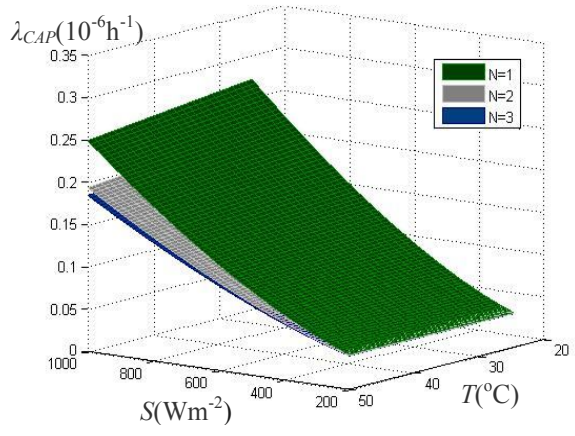


Fig. 3. Capacitor failure rate as a function of number of phases

The impact of voltage rating and capacitance on $\lambda_{CAP}$ for a two-phase converter is depicted in Fig. 4. While $\lambda_{CAP}$ increases with higher capacitance values, it decreases with voltage rating.

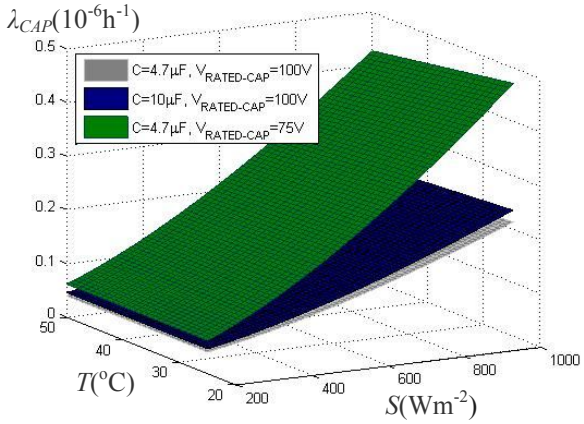


Fig. 4. Capacitor failure rate as a function of capacitance and voltage rating

## B. Diodes

The variation of diode failure rate, $\lambda_{DIODE}$, with voltage rating, $V_{RATING\text{-}DIODE}$, is depicted in Fig. 5. Apart from the obvious observation of improved reliability with increased voltage rating, notice that $\lambda_{DIODE}$ is more sensitive to temperature, as compared to $\lambda_{CAP}$. Additionally, for a given insolation, $\lambda_{CAP}$ is inversely proportional to temperature, while $\lambda_{DIODE}$ is directly proportional.

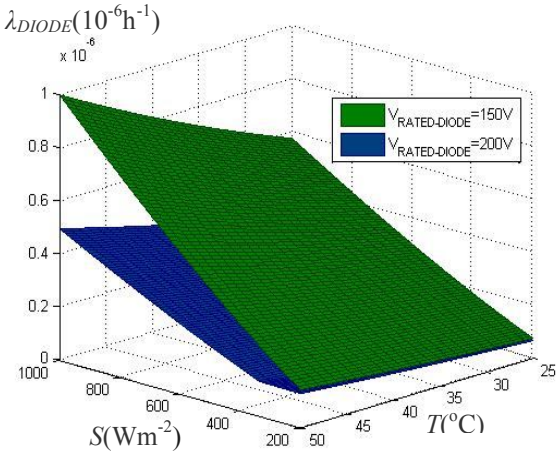


Fig. 5. Diode failure rate as a function of voltage rating

## C. Active switch

The conduction losses in the switch severely impair reliability across all ambient conditions. This is illustrated in Fig. 6, which depicts the variation of the switch failure rate, $\lambda_{SW}$, with switch resistance, $r_{SW}$. Notice also, the increased sensitivity of $\lambda_{SW}$ to temperature as compared to $\lambda_{CAP}$. Additionally, as with $\lambda_D$, $\lambda_{SW}$ increases with temperature as opposed to $\lambda_{CAP}$.

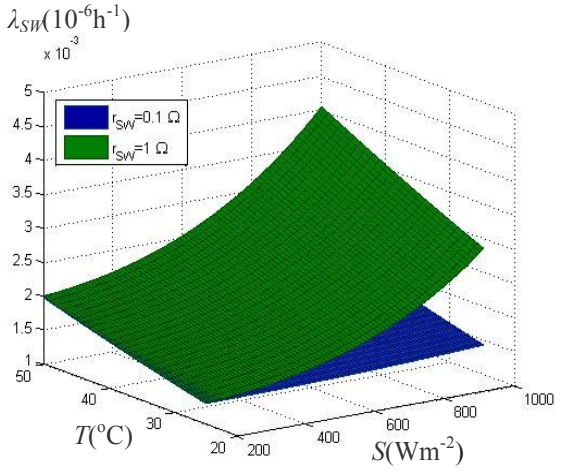


Fig. 6. Switch failure rate as a function of resistance

## IV. Markov Reliability Model

Component failure rates are noted to be functions of operational conditions, including but not limited to the number of phases, insolation, temperature, and device ratings. This precludes the possibility of using a combinatorial approach to reliability assessment. Unfortunately, while insolation and temperature vary with time, we can not necessarily reflect this in the failure rates. One possible option then is to design for worst-case ambient conditions, while acknowledging the dependence of failure rates on topology. A Markov reliability model serves this method best, as the model could be designed to accommodate state-dependent failure rates.

For an $N$-phase converter, ideally, all phases and output capacitors are operational. However, the converter could function with a reduced number of phases and a depleted output capacitor bank. The failure of a switch, diode or inductor in each phase would take that phase out of operation but the capacitor bank could still serve its fundamental purpose of energy storage with just one capacitor.

As a matter of notation, we will refer to the input stage as that composed of the inductors, switches and diodes and the output stage will refer to the capacitor bank. This is depicted in Fig. 7.

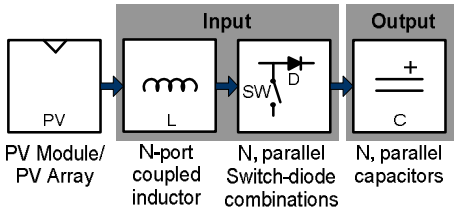


Fig. 7. Input and output stages highlighted

The state-transition diagram of an $N$-phase converter is shown in Fig. 8. The state $ij$ represents an $N$-phase converter operating with $i$ failed input stages and $j$ failed output stages. The failure rates of the switches and diodes in the converter are represented as $\lambda_{SW/Dx}$, $0 \le x \le N-1$, where $x$ represents the number of failed input phases. The failure rates of the capacitors in the output stage are of the form $\lambda_{CAPxy}$, $0 \le x \le N-1$, $0 \le y \le N-1$. The first index represents the number of failed input stages and the second, the number of failed output capacitors. Notice that the capacitor failure rates depend on both, the number of operational capacitors and switching devices.

With reference to the state transition diagram in Fig. 8, the failure rates corresponding to a transition from state $ij$ to $i(j+1)$ represent failures in the output stage (capacitor). The failure rate accompanying such a transition is of the form $(N-j)\lambda_{CAPij}$. Analogously, the failure rates corresponding to a transition from state $ij$ to $(i+1)j$ represent failure of an input stage (active switch or diode). The failure rate accompanying such a transition is of the form $(N-i)$ $(\lambda_{SWi} + \lambda_{Di})$. Transitions from states of the general form $(N-1)j$ to state $NN$ are at the rate $(\lambda_{SWi} + \lambda_{Di})$. Similarly, transitions from states of the general form $i(N-1)$ to state $NN$ are at the rate $\lambda_{CAPi(N-1)}$.

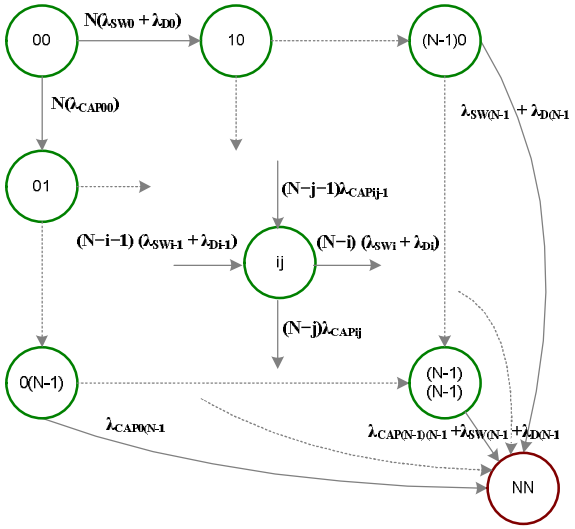


Fig. 8. State transition diagram of $N$-phase converter

The Laplace transform of the Chapman-Kolmogorov equations are solved to quantify system reliability [13]. The Laplace transform of the transition probability of a given state, $ij$, $P_{ij}(s)$, is computed as

$$P_{ij}(s) = \frac{(N-j-1)(\lambda_{CAPi(j-1)})}{[s+(N-j)\lambda_{CAPij}+(N-i)(\lambda_{SWi}+\lambda_{Di})]} P_{i(j-1)}(s) + \frac{(N-i-1)(\lambda_{SW(i-1)}+\lambda_{D(i-1)})}{[s+(N-j)\lambda_{CAPij}+(N-i)(\lambda_{SWi}+\lambda_{Di})]} P_{(i-1)j}(s) \quad (8)$$

The Laplace transform of the probability of the operational state, 00, can be expressed as:

$$P_{00}(s) = \frac{1}{[s + N(\lambda_{CAP00} + \lambda_{SW0} + \lambda_{D0})]} \quad (9)$$

The overall system reliability is quantified using the mean time to failure (MTTF). Since no repairs are included, the MTTF is more applicable as compared to the mean time between failures (MTBF), which would typically find application in describing the reliability of repairable systems. The MTTF of the system can be expressed as:

$$MTTF = \sum_{i=0}^{N-1} \sum_{j=0}^{N-1} P_{ij}(0) \quad (10)$$

The applicability of the derived Markov reliability model is demonstrated in the context of comparative studies for two- and three-phase, interleaved boost converters. The specifications of the converters and device ratings are the same as those documented in Table III. The variation of the MTTF for two- and three-phase converters as a function of switch resistance, $r_{SW}$, is depicted in Fig. 9. Surprisingly, an increase in $r_{SW}$ increases the MTTF. This is because, for a fixed impedance load, an increase in $r_{SW}$ reduces the output voltage. In turn, the stress on the output capacitors is reduced, making them more reliable. Since the capacitors dominate the reliability of the converter, the MTTF is increased.

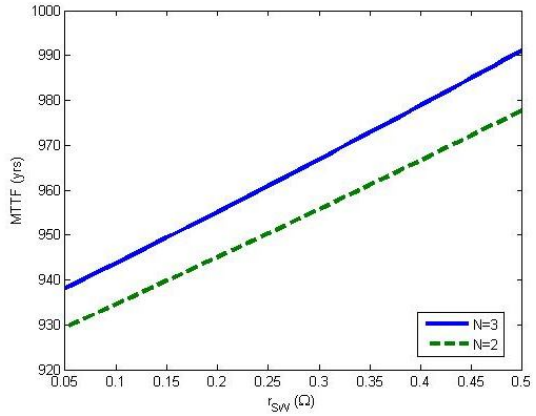


Fig. 9. MTTF as a function of switch resistance

A cursory comparison of the failure rates illustrated in Figs. 3-6 indicates that the capacitor failure rates are higher than that of the switches across all ambient conditions and design choices. Hence, the overall converter reliability is expected to be dominated by the output capacitors. Towards this end, we consider the impact of the voltage rating of the capacitors, $V_{RATING\text{-}CAP}$, on the MTTF of two- and three-phase converters. As Fig. 10 indicates, the MTTF is much more sensitive to $V_{RATING\text{-}CAP}$ than $r_{SW}$.

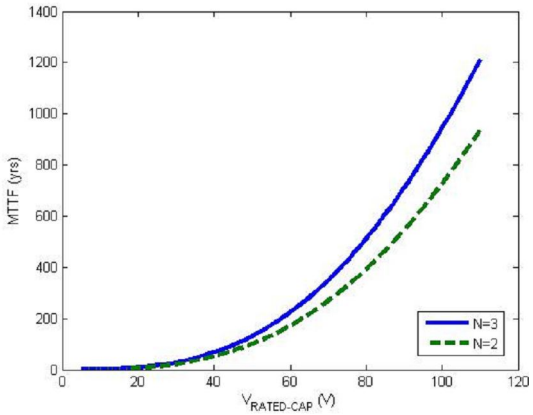


Fig. 10. MTTF as a function of capacitor voltage rating

Fig. 11 investigates the impact of the choice of capacitance on the MTTF of two- and three-phase converters. For a fair comparison, in this case study and the next, the capacitors in the two-phase converter are rated for 110 V while those in the three-phase converter are rated for 100 V. This ensures a fair comparison in that, for the base case specifications attached in Table III, the MTTF of the two converters is almost the same. The results illustrate that for each converter, there is an optimal capacitance value that maximizes the MTTF. Also, note that topological redundancy does not necessarily guarantee improved reliability. For capacitances below 6 $\mu F$, the voltage stress tends to dominate $\lambda_{CAP}$, and a higher number of phases guarantee improved reliability. Beyond 6 $\mu F$, the degradation in the failure rate due to high capacitance and the higher voltage rating of the capacitors in the two-phase converter overshadow the voltage stress factor, making the two-phase converter more reliable.

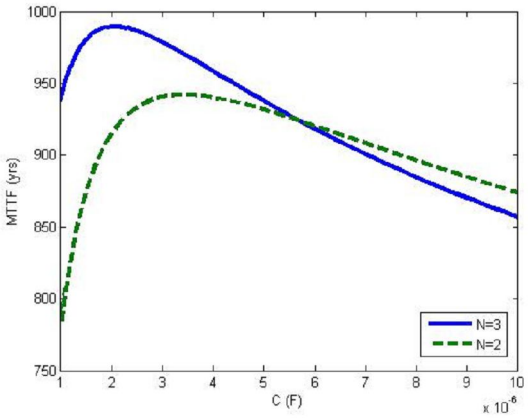


Fig. 11. MTTF as a function of capacitance

Finally, we consider the impact of switching frequency on the MTTF. The predominant effect is the reduction in output voltage ripple with higher switching frequencies. This

reduces the voltage stress on the output capacitors, hence extending their expected lifetime. Fig. 12 indicates that this effect is only valid up to 12 kHz. Beyond that, the higher

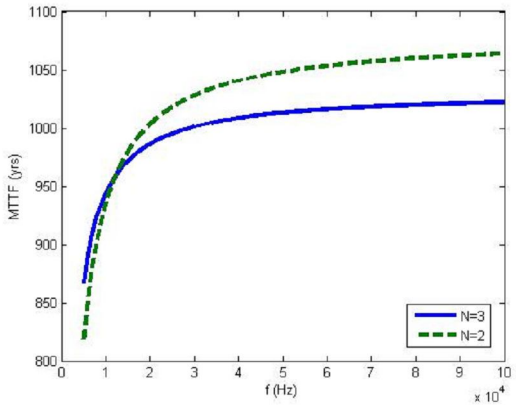


Fig. 12. MTTF as a function of switching frequency

voltage rating of the capacitors in the two-phase converter causes this topology to be more reliable across all possible switching frequencies.

## V. Conclusions

The proposed tools allow for rapid evaluation of reliability metrics of a fairly involved dc-dc converter topology intended for PV applications. For a constant impedance load, the output capacitors are noted to dominate the reliability of the converter. Future research may investigate the application of time-varying failure rates to the analysis. In addition, numerical optimization tools could suggest optimal converter specifications, given bounds on performance and reliability.

## References


[1] E. L. Meyer and E. E. van Dyk, "Assessing the reliability and degradation of photovoltaic module performance parameters," *IEEE Trans. on Reliability*, vol. 53, pp. 83-92, Mar. 2004.

[2] M. Vazquez and I. R.-Stolle, "PV module reliability model based on field-degradation studies," *Prog. Photovoltaic: Res. Appl.*, vol.16, pp.419-433, 2008.

[3] Y. C. Qin, N. Mohan, R. West and R. Bonn, "Status and needs of power electronics for photovoltaic inverters," Sandia National Labs., Jun. 2002. [Online]. Available: http://www.prod.sandia.gov/cgi-bin/techlib/access-control.pl/2002/021535.pdf

[4] N. G. Dhere, "Reliability of PV modules and balance-of-system components," in *Proc. 31st IEEE PV Spec. Conf.*, pp. 1570–1576, 2005.

[5] A. Ristow, M. Begovic, A. Pregelj and A. Rohatgi, "Development of a methodology for improving Photovoltaic inverter reliability," *IEEE Trans. Industrial Electronics*, vol. 55, pp. 2581-2592, Jul. 2008.

[6] A. Dominguez-Garcia and P. T. Krein, "Integrating reliability into the design of fault-tolerant power electronics systems," in *Proc. 2008 IEEE Power Electronics Specialist Conference*, pp. 2665-2671.

[7] H. Calleja, F. Chan and I. Uribe, "Reliability-oriented assessment of a Dc/Dc converter for Photovoltaic applications," in *Proc. 2007 IEEE Power Electronics Specialist Conference*, pp. 1522-1527.

[8] F. Chan, H. Calleja, and E. Martinez, "Grid connected PV systems: A reliability-based comparison," in *Proc. 2006 IEEE International Symposium on Industrial Electronics*, pp. 1583–1588.

[9] F. Chan and H. Calleja, "Reliability: A new approach in design of inverters for PV systems," in *Proc. 10th IEEE International Power Electronics Congress*, 2006, pp. 1–6.

[10] SPR-230-WHT, Sunpower 230 Watt PV Module data sheet [Online]. Available: http:// www.sunpowercorp.com

[11] S. V. Dhople, A. Davoudi and P. L. Chapman, "Steady-state characterization of multi-phase, interleaved dc-dc converters for Photovoltaic applications," presented at the inaugural IEEE Energy Conversion Congress and Exposition, 2009.

[12] Reliability Prediction of Electronic Equipment. Department of Defense, MIL-HDBK-217F, Jan. 1990.

[13] M. Rausand and A. Høyland, *System Reliability Theory*. Hoboken, NJ: Wiley, 2004.